THE ASTRONOMICAL JOURNAL VOLUME 86, NUMBER 10 OCTOBER 1981

COMET BRADFIELD 1979 X: THE GASSIEST COMET?

MICHAEL F. A'HEARN
Astronomy Program, University of Maryland, College Park, Maryland 20742

ROBERT L. MILLIS[a]
Lowell Observatory, Flagstaff, Arizona 86002

PETER V. BIRCH
Perth Observatory, Perth, Australia

Received 16 April 1981; revised 15 July 1981

ABSTRACT

We present the results of narrowband filter photometry of Comet Bradfield 1979 X for post-perihelion, heliocentric distances from 0.57 to 1.65 AU. The emission-to-continuum ratio was found to be larger than that for any other comet measured by us, including P/Encke, although much of the "continuum" in both comets is probably due to weak emission features. A sharp change in this ratio observed at 0.85 AU is attributed to the sudden appearance of an emission feature in our continuum bandpass. For the first time, we present OH production rates obtained contemporaneously with the production rates of the species more usually observed from the ground. All molecular species show a very steep variation with heliocentric distance, averaging about $r_H^{-3.2}$. This appears inconsistent with simple models of vaporization equilibrium and suggests that other factors, such as an insulating mantle or chemical reactions in the coma, may be important in controlling the gas production of this comet. There appear to be changes in the relative production rates with heliocentric distance in the sense that the comet was very CN-rich for a short time at discovery (heliocentric distance 0.5 AU post-perihelion), then became "normal" from 0.6 to 1.0 AU, and gradually became somewhat CN-rich at heliocentric distances beyond 1 AU.

I. INTRODUCTION

As part of our long-range program to obtain quantitative photometric data on a large number of comets, we sometimes are able to observe individual comets over a wide range of heliocentric distances. Observations of this type are valuable for understanding the vaporization process of the nucleus, i.e., for determining the nuclear surface structure and composition, and for constraining the dominant production mechanisms for various chemical species in the coma. Comet Bradfield 1979 X was the most recent such opportunity. Although this comet was not an unusually luminous one, its very close approach to Earth enabled us to observe it from the time of discovery at a heliocentric distance of just over 0.5 AU until it was beyond 1.5 AU from the Sun.

II. OBSERVATIONS AND DATA REDUCTION

In general, the photometric techniques employed were identical to those used by us previously (cf. A'Hearn and Millis 1980, and other references therein). Because of the unusual geometry of this apparition, wherein the comet moved very rapidly from far southerly declinations to moderate northern declinations near the time of closest approach to Earth, all of the early observations (from 28 December 1979 through 20 January 1980) were made from Perth Observatory using the 24-in. Planetary Patrol Telescope. From 29 January through 12 February we obtained data with an identical Planetary Patrol Telescope at Mauna Kea Observatory, while on 1 and 2 February as well as on 9 and 10 March we observed Comet Bradfield with the 42-in. telescope at the Lowell Observatory. At Perth, the filters used were identical to those we have described previously (A'Hearn, Millis, and Birch 1979) and which have been used in our previous work. At Mauna Kea and Lowell the filters for CN, C_3, and C_2 are the same ones that we have used previously, but we have added filters to isolate the emission bands of OH at 3085 Å and of NH at 3365 Å. We have also added continuum filters at 3300 and 3675 Å, the first in order to provide a continuum point nearer OH, and the second to provide a purer continuum than was available with our previous filters. To accommodate these new filters in the photometers, it was necessary to eliminate two of our previous continuum filters at 3930 and 4120 Å although we have retained our original continuum filter at 5240 Å. The characteristics of the four new filters are given in Table I. The results with the NH filter will not be discussed here because the profile of the band and the fluorescence efficiency are expected to be strong functions of the heliocentric radial velocity owing to the Swings effect and this problem is still being studied (M. Litvak 1980, private communication).

The data reduction for the observations of OH is complicated by a number of factors, several of them due to

[a]Guest Observer, Mauna Kea Observatory, Institute for Astronomy, University of Hawaii.

 0004-6256/81/101559-08$00.90

TABLE I. Characteristics of new filters.

Feature isolated	Center wavelength (Å)	Bandpass FWHM (Å)	Transmission at peak (%)	Manufacturer
OH ($A\,^2\Sigma$–$X\,^2\Pi$; $\Delta v = 0$)	3135 (peak at 3099)	170	28	Spectro Film
Continuum	3292	49	29	Spectro Film
NH ($A\,^3\Pi$–$X\,^3\Sigma$; $\Delta v = 0$)	3372	67	37	Spectro Film
Continuum	3672	60	33	Micro Coatings

the limitations of the filters we used, which have asymmetric profiles with centroids located significantly longward of the peak. The atmospheric attenuation at these wavelengths is produced by three, discrete components: aerosol scattering, Rayleigh scattering, and ozone absorption, of which the first is very small compared to the others. Our observations of atmospheric attenuation and comparisons with some theoretical calculations have already been presented (Millis and A'Hearn 1981) but further understanding has now been achieved and we discuss these results in some detail.

The general approach has been described, for example, by Festou (1981b) in the context of his photographic observations of OH. Theoretical calculations of the monochromatic extinction coefficients have been made using the formulas of Hayes and Latham (1975) together with ozone column densities from Allen (1963) and ozone absorption coefficients from Toolin (1965). We note that Mauna Kea exhibits much less Rayleigh scattering than does Lowell because of its much higher altitude (4.2 km vs 2.2 km) but it also exhibits less ozone absorption because the ozone column density varies with latitude (as well as season), being 20% smaller at the latitude of Mauna Kea than at the latitude of Flagstaff. We have used these monochromatic extinction coefficients to calculate the effective extinction for a star with a flat spectrum observed through our filters. We find that the filters are sufficiently wide so that extinction is very nonlinear with air mass because the effective wavelength changes markedly with extinction. Although the calculated effective extinction coefficients are very different for the two sites (e.g., 1^m134 at MKO vs 1^m407 at Lowell for 1 air mass), the deviations from linearity are nearly identical at the two sites, the extinction at two air masses being 1.851 times that at one air mass. Because the deviations from linearity are independent of the actual extinction, we use them to define an effective air mass, with which the observed magnitude is expected to vary linearly, and we then determine observationally, in the usual manner, an effective extinction coefficient which corresponds to the true extinction at one air mass and we correct our observations of standard stars to magnitudes outside the atmosphere using these effective air masses and extinction coefficients. Table II shows the results of our extinction observations in the best-determined cases compared with the theoretical calculations for "average" conditions. The small, systematic difference between theory and observation is of no importance because theory is used only for determination of the nonlinearities.

Because the OH spectrum of the comet does not resemble the stellar spectrum, the extinction coefficient for the comet is also different from that for stars. We have used theoretically calculated fluorescence spectra of the 0–0 and 1–1 bands of OH (see below) to calculate theoretical extinction coefficients for the cometary observations. Because the OH bands are dominated by a few strong lines with effective wavelength 3086 Å, all located within 10 Å of the effective wavelength, the observed cometary magnitude is nearly linear with air mass but the extinction coefficients for the comet are much larger than those for stars. Because the stellar ef-

TABLE II. Stellar extinction coefficients for OH filter.

Date	$k(X=1)$[a]	Mauna Kea Air mass range	Eff. air mass range[b]	Date	$k(X=1)$[a]	Lowell Air mass range	Eff. air mass range[b]
theory	1.134			theory	1.407		
29 Jan	1.057 ± 0.006	1.17–3.35	1.15–2.89	2 Feb	1.304 ± 0.005	1.74–3.41	1.69–2.98
30 Jan	1.122 ± 0.037	1.12–2.65	1.10–2.28				
5 Feb	1.098 ± 0.005	1.05–2.86	1.05–2.52				
8 Feb	1.080 ± 0.012	1.62–3.12	1.54–2.72				
12 Feb	1.031 ± 0.004	1.07–3.92	1.06–3.30				

[a]Effective extinction coefficient = total extinction (mag) at 1 air mass.
[b]Effective air mass = variable with which extinction should be linear and to which effective extinction coefficient corresponds.

TABLE III. Observational data for Comet Bradfield 1979 X.

1979-80	r_H [AU]	Δ [AU]	ϕ[a] [deg]	Diaphragm[b] [arcsec]	V[e]	log F[c] OH	CN	C_3	C_2	log F_λ[c] (contin) λ3300	λ3675	λ3930	λ4120	λ5240	$W_\lambda(C_2)$[d] [10^3 Å]
						Observations from Perth									
1979															
Dec 28.83	.570	1.082	65	155 P	5^m.87	--	-7.607	-9.297	-7.923	--	--	-11.23	-11.38	-12.06	14
							±.08	±.10	±.02			±.08	±.04	±.17	
Dec 29.82	.577	1.048	67	"	5.85	--	-7.773	-9.916	-7.903	--	--	-11.17	-11.24	-11.88	9.5
							±.01	±.03	±.03			±.02	±.01	±.12	
1980															
Jan 2.81	.613	.909	78	"	6.00	--	-8.018	-9.386	-7.970	--	--	-11.28	-11.44	-12.17	16
							±.02	±.03	±.01			±.03	±.01	±.12	
Jan 3.82	.623	.874	80	"	5.92	--	08.011	-9.329	-7.952	--	--	-11.28	-11.44	-12.20	18
							±.01	±.05	±.02			±.02	±.01	±.18	
Jan 7.81	.671	.729	89	"	6.10	--	-8.160	-9.128	-8.061	--	--	-10.98	-11.49	-12.24	15
							±.01	±.02	±.01			±.01	±.02	±.09	
Jan 9.82	.697	.655	93	"	6.27	--	-8.238	-9.394	-8.108	--	--	-11.40	-11.57	-12.25	14
Jan 10.80	.710	.620	95	"	6.31	--	-8.241	-9.379	-8.099	--	--	-11.42	-11.60	-12.31	16
Jan 13.83	.754	.510	100	"	6.57	--	-8.383	-9.381	-8.268	--	--	-11.47	-11.78	--	
							±.01	±.01	±.03			±.01	±.01		
Jan 16.80	.798	.406	105	"	6.75	--	-8.483	-9.319	-8.278	--	--	-11.43	-11.68	-12.56	(43)
							±.02	±.04	±.02			±.02	±.03	±.25	
Jan 17.82	.814	.372	106	"	6.76	--	-8.474	-9.285	-8.277	--	--	-11.43	-11.64	-12.55	19
							±.01	±.02	±.01			±.01	±.01	±.15	
Jan 18.83	.829	.339	107	"	6.92		-8.471	-9.308	-8.295	--	--	-11.41	-11.55	-12.63	22
							±.01	±.01	±.01			±.01	±.01	±.14	
Jan 20.81	.860	.280	108	"	7.06	--	-8.583	-9.246	-8.396	--	--	-11.44	-11.68	-12.24	6.3
						Observations from Mauna Kea and Flagstaff									
Jan 29.29	.996	.239	80	111 M	--	-8.424	-9.128	-9.641	-9.002	-12.50	-12.16	--	--	-12.74	5.5
Jan 30.27	1.012	.262	77	111 M	--	-8.564	-9.180	-9.737	-9.047	-12.59	-12.18	--	--	-12.81	5.8
						±.02	±.02	±.05	±.01	±.04				±.01	
Feb 1.12	1.042	.314	71	98.8 F	--	-8.655	-9.404	-9.979	-9.176	-12.86	-12.37	--	--	-13.44	(18.)
						±.02	±.02	±.06	±.02	±.10	±.02			±.50	
Feb 2.13	1.059	.345	68	98.8 F	--	-8.699	-9.422	-9.997	-9.226	-12.69	-12.35	--	--	-13.01	6.1
						±.02	±.01	±.02	±.01	±.05	±.01			±.08	
Feb 2.20	1.060	.348	68	60.3 F	--	-9.066	-9.732	-10.229	-9.574	< -13	-12.90	--	--	(-15.35)	
Feb 5.28	1.110	.451	62	111 M	--	-8.889			-9.340	-12.79	-12.48	--	--	-13.05	5.1
						±.01	±.01	±.02	±.01	±.10	±.03			±.04	
Feb 6.25	1.126	.485	61	111 M	--	-8.929	-9.568	-10.198	-9.400	--	-12.69	--	--	-13.05	4.5
							±.01	±.01	±.01					±.01	
Feb 8.28	1.159	.557	58	111 M	--	-9.059	-9.675	-10.269	-9.516	--	-12.74	--	-12.62	-13.14	4.2
						±.01	±.07	±.03	±.01		±.01		±.02	±.06	
Feb 9.28	1.176	.593	57	111 M	--	-9.154	-9.693	-10.313	-9.557	--	-12.80	--	-12.69	-13.30	5.6
						±.01	±.02	±.03	±.02		±.02		±.01	±.03	
Feb 12.28	1.224	.702	54	111 M	--	-9.237	-9.803	-10.452	-9.655	--	-12.86	--	-12.76	-13.37	5.2
						±.01	±.02	±.03	±.01		±.01		±.02	±.04	
Mar 9.16	1.633	1.633	35	53.5 F	--	--	-11.003	-11.628	-10.957	--	--	--	--	-14.46	3.2
							±.02	±.09	±.04					±.08	
Mar 10.13	1.648	1.666	35	53.5 F	--	--	-10.993	-11.758	-10.956	--	--	--	--	-14.41	2.9
							±.02	±.19	±.04					±.10	

Notes: a. Phase angle = sun-comet-earth angle.
b. Diameter of diaphragm projected on sky; letters P,M,F indicate observations from Perth, Mauna Kea, and Flagstaff, respectively.
c. Emission band fluxes in [erg - cm^{-2} - s^{-1}]; continuum fluxes in [erg - cm^{-2} - s^{-1} - $Å^{-1}$] are average, fluxes over the continuum filter bandpasses and may be dominated by weak emission features rather than true continuum .
d. Equivalent width of Δv=0 sequence of C_2 Swan bands. Normally this is a measure of the gas-to-solids ratio but in this case it is just an upper limit.
e. V magnitude as measured through the indicated diaphragm.

fective wavelength is so far from the cometary effective wavelength (which is nearly at the peak of the filter profile), this ratio of cometary to stellar extinction coefficients varies slightly from site to site, being 1.229 at MKO and 1.244 at Lowell. We use these theoretically calculated ratios to determine extinction coefficients for the cometary observations from our observational results for the standard stars. On nights when we have several cometary observations at different air masses, the resultant magnitudes corrected for atmospheric extinction agree with each other to within $\pm 0^m.01$, which implies that our method of determining extinction is reliable.

The stellar calibration was obtained from the ultraviolet fluxes of η UMa given by Code and Meade (1979). These were transferred to μ Tau, the brightest of our standard stars, by an extrapolation of the magnitude differences between μ Tau and η UMa given by Breger (1976).

As has been known for many years (e.g., Hunnaerts 1953), the OH bands show a very pronounced Swings effect, with both the relative line strengths and the total flux in the bands varying strongly with heliocentric radial velocity. Because previous authors have published results only for particular radial velocities of interest, a complete set of band profiles and fluorescence efficien-

TABLE IV. Parameters for reduction of fluxes to production rates.

Species	Emission feature	log g (erg s^{-1})	Parent scale length (km)	Daughter scale length (km)
C_2 triplets	$d\,^3\Pi_g$–$a\,^3\Pi_u$; $\Delta v = 0$	– 12.657	$1.7 \times 10^4\ r_H^1$	$1.2 \times 10^5\ r_H^2$
C_3	$^1\Pi_u$–$^1\Sigma_g{}^+$	– 13.60	$1.0 \times 10^3\ r_H^2$	$5.4 \times 10^4\ r_H^2$
CN	$B\,^2\Sigma^+$–$X\,^2\Sigma^+$; $\Delta v = 0$	a	$2.19 \times 10^4\ r_H^2$	$3.0 \times 10^5\ r_H^2$
OH	$A\,^2\Sigma^+$–$X\,^2\Pi$; $\Delta v = 0$	b	$4.1 \times 10^4\ r_H^2$	$1.16 \times 10^5\ r_H^2$

[a]Varies with $\dot{r}_H$; $1/g$ is ordinate of Fig. 1 of Tatum and Gillespie (1977) times $4\pi \times 10^7$; values used here range from – 12.245 to – 12.418.
[b]Varies with $\dot{r}_H$ (Schleicher and A'Hearn 1981); flux is > 95% from 0–0 band; values used here range from – 14.244 to – 14.247.

cies has been calculated as a function of radial velocity (Schleicher and A'Hearn 1981). The profiles for the appropriate radial velocities of Comet Bradfield have been used to convert our observed fluxes through the filters to total emission-band fluxes.

The resultant band and continuum fluxes derived from all observations are given in Table III. Where errors are quoted, they represent the standard deviation due purely to photometric uncertainty and are thus a measure of the precision, not the absolute accuracy, of the results. Over the last year we have also observed numerous solar-type stars through our filters. These enable us to predict the magnitudes that we would observe in the emission-band filters in the absence of any emission bands and thus provide an alternative method for subtracting the continuum from the emission-band measurements. For a comet with high emission-to-continuum ratio such as Bradfield, this approach gives identical emission-band fluxes. The largest source of error is from extraneous weak emission features within our bandpasses. These can lead to errors of several percent in the emission-band fluxes and, as discussed below, can dominate the "pseudo-continuum" fluxes for a gasssy comet such as Bradfield.

The total number of molecules in the field of view has been derived from the general formula

$$\log M(\rho) = \log F(\rho) + 27.449 + 2 \log r\Delta + \log g,$$

where F is the band flux in cgs units, r and Δ are in AU, and g is the fluorescence efficiency per molecule at $r = 1$ AU as given in Table IV. The constant represents the surface area of a sphere of radius = 1 AU and ρ the radius of the observed column at the comet. The fluorescence efficiency of OH, as noted above, has been taken

TABLE V. Column densities and production rates.

1979-80 UT Date	r_H [AU]	ρ[a] [10^4km]	log M(ρ)[b] OH	CN	C_3	C_2	log Q[c] OH	CN	C_3	C_2
Dec 28.83	.570	6.07	--	31.67	31.33	31.76	--	26.95	27.05	27.26
29.82	.577	5.88	--	31.53	31.30	31.77	--	26.82	27.00	27.27
Jan 2.81	.613	5.07	--	31.28	31.16	31.63	--	26.61	26.83	27.13
3.82	.623	4.90	--	31.27	31.19	31.63	--	26.60	26.86	27.13
7.81	.671	4.09	--	31.03	31.30	41.42	--	26.43	26.94	26.96
9.82	.697	3.68	--	30.87	30.98	31.32	--	26.31	26.61	26.88
10.80	.710	3.48	--	30.83	30.96	31.30	--	26.30	26.59	26.88
13.83	.754	2.87	--	30.58	30.84	31.01	--	26.15	26.49	26.66
16.80	.798	2.28	--	30.35	30.75	30.85	--	26.05	26.43	26.61
17.82	.814	2.09	--	30.31	30.73	30.79	--	26.06	26.43	26.60
18.83	.829	1.90	--	30.25	30.64	30.71	--	26.06	26.36	26.56
20.81	.860	1.57	--	30.01	30.57	30.47	--	25.95	26.34	26.44
29.29	.996	0.96	32.02	29.49	30.16	29.86	28.57	25.81	26.10	26.14
30.27	1.012	1.05	31.98			29.91	28.47	25.78	26.09	26.14
Feb 1.12	1.042	1.13	32.07	29.49	30.10	29.96	28.53	25.73	25.97	26.15
2.13	1.059	1.24	32.12	29.57	30.18	30.01	28.53	25.75	26.01	26.14
2.20	1.060	0.76	31.76	29.27	29.95	29.66	28.50	25.78	25.98	26.12
5.28	1.110	1.82	32.21	29.77	30.30	30.16	28.37	25.72	25.98	26.07
6.25	1.126	1.95	32.24	29.77	30.33	30.18	28.37	25.68	25.98	26.04
8.28	1.159	2.24	32.26	29.83	30.40	30.21	28.30	25.66	26.00	25.99
9.28	1.176	2.40	32.23	29.86	30.42	30.24	28.24	25.65	26.00	25.98
12.28	1.224	2.83	32.32	29.93	30.47	30.32	28.22	25.63	25.98	25.97
Mar 9.16	1.633	3.17	--	29.67	30.27	30.00	--	25.42	25.70	25.61
10.13	1.618	3.23	--	29.70	30.17	30.03	--	25.45	25.59	25.63

Notes
a. Projected radius of diaphragm at comet.
b. Column densities integrated over the radius indicated in column 3, i.e. total number of molecules in the observed volume.
c. Production rates in radicals per second assuming a lifetime [s] equal to the scale length [km]. In a pure Haser model, this corresponds to an expansion velocity of 1 km-s^{-1}.

from complete calculations of the fluorescence equilibrium of OH. It varies by a factor of 7 for the range of velocities encountered for all comets but varies only slightly for the range of radial velocities of Comet Bradfield during the observations. The fluorescence efficiencies for the other species have been discussed in our previous papers and are summarized in Table IV. The resultant integrated column abundances are given in Table V.

Because the observations correspond to a wide range of volumes in the comet, it is desirable to convert the observed numbers of molecules into a quantity that can be used to make direct comparisons among various, observational data. Although the Haser model has been much criticized in recent years for being physically unrealistic, it still provides a useful mathematical framework for converting the number $M(\rho)$ of molecules in a particular column, where ρ is the radius of the observed column, to the total number M of molecules in the coma. The values of the two scale lengths of the Haser model are all one needs to carry out this extrapolation with reasonable accuracy. Provided the observed column is reasonably large compared to the scale lengths, the result is not very model dependent, i.e., even if the fit of the Haser model is not very good, one still can get a reasonably good estimate of M. This total number can then be directly converted to a production rate by dividing it by the lifetime of the species in question. This result becomes strongly model dependent only if one associates the Haser-model scale length directly with the lifetime.

Festou (1981a) has developed a vectorial model which allows for the nonradial velocity imparted to the OH radical when it is formed by photodissociation. This model yields surface brightness distributions which resemble those of a standard Haser model. Combi and Delsemme (1980a) have provided a simple method for relating the "true" scale length of the observed radicals in Festou's vectorial model to the effective, Haser-model scale length that describes the same distribution of surface brightness. For the cases of CN (Combi and Delsemme 1980b) and of OH (Festou 1981b) the differences between the true and effective scale lengths are not large. For C_2 and C_3, which may be produced by chemical reactions rather than by dissociation (e.g., Giguere and Huebner 1978), the situation is much more complex but we note that there is no agreement on a better approach to obtaining a production rate. In any case, the true lifetimes for any of these species are very uncertain. For these reasons, we continue to arbitrarily assume that the lifetimes (s) are equal to the effective Haser-model scale lengths (km). In the context of the original Haser model, this is equivalent to assuming an expansion velocity of 1 km/s, while in the context of Festou's vectorial model it is equivalent to assuming slightly larger velocities. The numerical values of the scale lengths used in our calculations are given in Table IV and the deduced production rates are given in Table V.

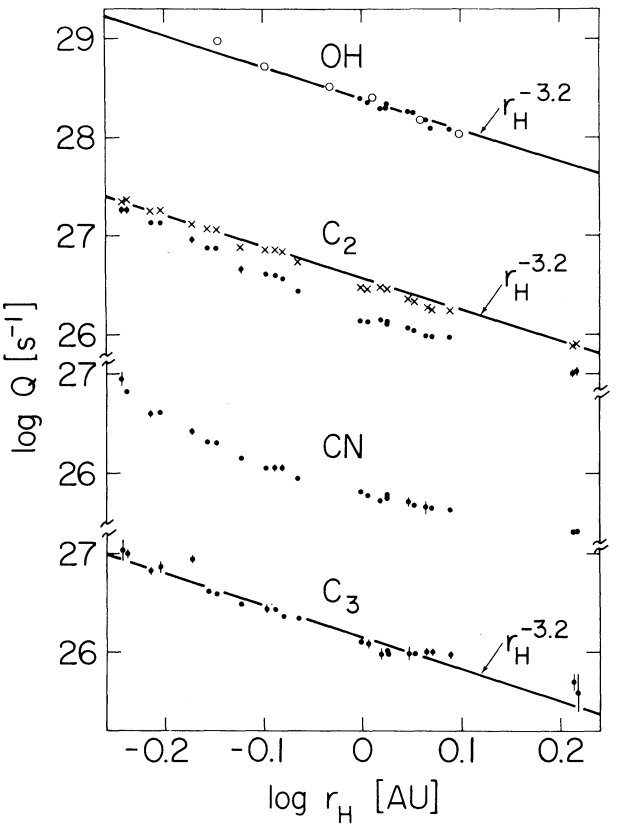

FIG. 1. Molecular production rates in Comet Bradfield 1979 X. Closed circles are ground-based data given in Table V. Open circles are results for OH obtained with IUE (Weaver *et al.* 1981). "×" symbols represent C_2 production assuming a parent scale length three times larger than standard. Straight lines have been fitted by eye for illustrative purposes.

III. DISCUSSION

In Fig. 1 we have plotted the various molecular production rates as a function of heliocentric distance. For comparison, we have also plotted the production rate of OH as determined from the IUE spacecraft (Weaver *et al.* 1981). The IUE results plotted here are lower than the results given by Weaver *et al.* (their case B Haser model) by the 90% conversion efficiency from H_2O to OH and by the 15% difference in OH lifetimes between this paper and that of Weaver *et al.* The effective Haser-model scale lengths used here for OH are the ones determined by Weaver *et al.* (their case B) so that both sets of data were reduced identically. The agreement is excellent considering the difference in technique. This agreement gives us confidence that we have correctly allowed for all atmospheric effects and that ground-based photometry of the OH bands can be obtained routinely without detailed calculations of the extinction for every night. Because the apertures used in our photometers (typically several arcminutes) are large compared to those used in IUE (10×15 arcsec), the agreement be-

tween the two types of data also confirms the choice of effective, Haser-model scale lengths of OH. The scale lengths used for the other species have been discussed previously (A'Hearn and Cowan 1980).

Perhaps the most striking feature of the heliocentric distance variation of the production rates is that, for all species, the variation is remarkably steep. This steep slope is in definite contrast to what was observed in Comet West (A'Hearn, Thurber, and Millis 1977), where the production rates were basically proportional to r_H^{-2}. That result could easily be understood in terms of equilibrium vaporization of an icy nucleus, with grains of water ice invoked to explain the "turn-off" of C_2 production beyond 1.5 AU (cf. A'Hearn and Cowan 1980). The results for Comet Bradfield cannot be understood in terms of such a simple model. We also note in passing that none of the data can be adequately represented by a variation with $\sqrt{r}$ as predicted by the desorption model of Levin (1966). An initial look at the "seasonal" effects expected if the comet has its rotation axis in its orbit plane (cf. Cowan and A'Hearn 1979) suggests that this effect is not sufficient to explain the observations, but this question requires further investigation. An alternative explanation involves the gradual exhaustion of an outer "frosting" of relatively volatile material as suggested by several authors. Whipple (1978) has discussed such a model to explain Comet Kohoutek. The major difficulty in applying such a model to Comet Bradfield is that the source of the frosting is generally thought to be associated with a long residence time in the Oort cloud, whereas Comet Bradfield has an orbital period of only approximately 300 yr. More plausible models involve either a heterogeneous surface or the buildup of an insulating crust as discussed, for example, by Whipple (1978) and modeled in more detail by Brin and Mendis (1979).

It is clear from Fig. 1 that OH and C_3 production can be represented adequately by a simple power-law variation. The straight lines in Fig. 1 have been fitted by eye and are arbitararily forced to have the same slope, viz. $r_H^{-3.2}$. The exponents are not reliable to better than ± 0.5, and, in fact, Weaver *et al.* (1981) obtained an exponent of -3.7 which fits the IUE data somewhat better than $r^{-3.2}$ shown here. Other species do not show such a simple variation.

The production rate of C_2 appears to follow two different power laws, with a change in exponent in late January. This change in slope, however, is concurrent both with the change in observing location and equipment and with the time of closest approach to Earth. The concurrence with closest approach suggests a possible problem in the choice of scale lengths. Because the scale length of the parent of C_2 is very uncertain and because this most seriously affects the surface brightness of the inner coma, this is the most likely candidate for change. We have therefore derived C_2 production rates using a variety of parent scale lengths, including in particular a parent scale length three times our usual

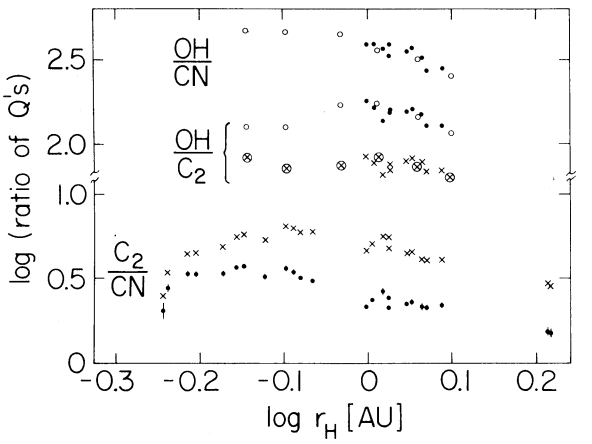

FIG. 2. Ratios of production rates in comet Bradfield 1979 X. Symbols are as in Fig. 1.

value, i.e., $5.1 \times 10^4 r_H^{+1}$ km. We have plotted the results for this case in Fig. 1 also to show how much the production rate changes for this large change in scale length. As shown, the results are then very well fit by a simple power law, $r_H^{-3.2}$. Such a large scale length for the parent of C_2 has been suggested by Combi (1978). On the other hand, recent work by Newburn (1981, private communication) on other comets suggests that our originally adopted scale length is nearly correct. Huebner (1981) has pointed out that, in chemical models of the coma, C_2 is one of the species that show a profile distinctly different from that of a Haser model. We suggest, therefore, that the apparent change of slope in the curve of C_2 production should be treated with caution and some skepticism. If the effect is real, it may be one of the few pieces of direct evidence for production of C_2 by means of density-dependent chemical reactions (Giguere and Huebner 1978; Mitchel *et al.* 1981).

We note that the visual magnitude of the comet, which is dominated by the Swan bands, exhibited a change in slope similar to that seen here for the C_2 production (Morris 1980). As was pointed out by Opik (1963) and discussed particularly for this comet by Morris (1980) and Marcus (1980), visual and photographic magnitudes are expected to show such effects correlated with geocentric distance owing to the fact that the eye (or photograph) integrates over a varying fraction of the comet. An error in our Haser-model parameters causes an analogous effect in our photometry. As noted above, the Haser-model parameters are sufficiently well known to correct for this effect in most cases. The unusually large variation in the geocentric distance of Comet Bradfield makes these observations unusually susceptible to uncertainties in the Haser-model parameters. Whether this effect of geocentric distance is the correct explanation or not will remain uncertain until the spatial distribution of C_2 is better determined in a variety of comets.

The variation of CN production is rather different.

The data exhibit a definite curvature. It is clear that, at the time of the comet's discovery, CN was being produced much more rapidly, compared to other species, than for most of the period of observation. This is clearly seen in Fig. 2, where we have plotted ratios of production rates. The increase in the C_2/CN ratio over the first several days of observation was far larger than could be explained by the photometric uncertainties. Neither can it be explained by any plausible changes in the scale lengths for CN or C_2 or their parents. There also appears to be a later, systematic, slow decrease in the C_2/CN ratio. If we again increase the scale length of the C_2 parent by a factor of 3, much of the decrease disappears, as is also shown in Fig. 2, but some decrease is still present. The rapid increase in the C_2/CN ratio just after discovery might be associated with the termination of a CN-rich flare at discovery while the turnover at large heliocentric distance might be associated with the cessation of H_2O vaporization as observed in Comet West by A'Hearn, Thurber, and Millis (1977) and modeled by A'Hearn and Cowan (1980).

In this respect, it is unfortunate that our observations of OH covered only a portion of the range in heliocentric distance. We have plotted the OH/C_2 and OH/CN production-rate ratios in Fig. 2 using both the C_2 production derived with standard parameters and the C_2 production derived with the increased parent scale length. To extend the range of the OH observations, we have again included the results from IUE. Over the limited range of our ground-based data, the ratio of production rates, OH/C_2, appears to be nearly constant. The OH data from IUE suggest that the OH/C_2 production-rate ratio is constant if one accepts the longer parent scale length but, if one accepts our "normal" scale lengths, the OH/C_2 ratio goes through a maximum near $r_H = 1$ AU. Whichever scale length one chooses, the C_2 production is about 1% that of OH. As A'Hearn and Millis (1980) have noted, the average ratio for many comets based on photometry for C_2 and based on microwave measurements of OH by Despois *et al.* (1980) is nearer 2%. This difference is probably due to differences in the observational techniques used for determining OH production rather than to a true difference in the relative production rates. We cannot yet determine which of the two observational techniques is better calibrated. The OH/CN production-rate ratio shows a definite variation with heliocentric distance. It is nearly constant for $r_H < 1$ AU and drops gradually for $r_H > 1$ AU. This is qualitatively similar to the behavior discussed above for the C_2/CN ratio.

The gas-to-dust ratio of this comet is striking. Examination of the equivalent widths of the C_2 emission given in Table III shows that until 18 January the gas-to-dust ratio was higher for this comet than for any other comet we have ever observed. These equivalent widths are a factor of 3–4 greater than those observed for previous very gassy comets such as P/Encke and Kohler 1977 XIV (cf. A'Hearn and Millis 1980). Then on 20 January there was a dramatic decrease in this ratio by a factor of 3–4 and values comparable to those for other very gassy comets prevail for the remainder of the observations. The change does not appear to be related to the change in observing sites which occurred after the observation on 20 January since the values derived from the Mauna Kea and Flagstaff data agree well, both with each other and with the Perth result for 20 January. Furthermore, recent observations of other comets using the filters from Perth show no significant difference from observations with the other filter sets.

Examination of the continuum and emission-band fluxes shows that the change is due to a sudden increase in the continuum flux rather than a decrease in the emission-band flux. It must be remembered, however, that our continuum filters are very sensitive to the presence of weak emission features when the true continuum is also weak. Thus the change in our measured equivalent width of C_2 is probably due to the appearance (on 19 or 20 January) of an emission feature in the vicinity of 5240 Å rather than to an increase in the true continuum. In fact, examination of the continuum fluxes at 4120 Å shows no significant enhancement beginning on 20 January, also suggesting a weak emission feature rather than a change in the true continuum. This might well be an NH_2 emission band since the 0,12,0 and 1,8,0 bands of NH_2 both lie well within the bandpass of our filter at 5240 Å, while there are no strong NH_2 bands lying within the bandpass of our continuum filter at 4120 Å.

We have used the excess flux seen in our λ 5240 filter on 20 January to estimate the amount of NH_2 required to produce the excess. Using a crude profile expected for the 0,12,0 band of NH_2, we find that a band flux of 6×10^{-11} erg cm^{-2} s^{-1} would produce the observed excess. Using a fluroescence efficiency of 5.5×10^{-14} erg s^{-1} per radical at $r_H = 1$ AU (A'Hearn 1981), we find a total content for NH_2, $M(\rho) = 1.5\times10^{29}$, i.e., about 5% that for C_2. Since the C_2 has a much greater spatial extent than does NH_2, the required total NH_2 content of the coma is less than 5% that of C_2, i.e., somewhat less than estimated for previous comets with readily observable bands of NH_2 (cf. A'Hearn, Hanisch, and Thurber 1980). There is no obvious reason that NH_2, or any other species for that matter, should suddenly appear beyond this heliocentric distance. Clearly spectroscopic data for mid-January would be of great value in determining the cause of this sharp change in our measured equivalent widths.

IV. CONCLUSIONS

(1) The determination of the OH production of comets can be made routine, even at moderate altitudes.

(2) Comet Bradfield 1979 X was one of the gassiest comets ever observed, comparable to Comet P/Encke.

(3) It seems likely that an emission feature, possibly due to NH_2, was present at a wavelength near 5240 Å for $r_H > 0.85$ AU but not present at $r_H < 0.85$ AU.

(4) The production rates of all molecular species

dropped sharply with heliocentric distance, more steeply than r_H^{-3}, in a way that seems inconsistent with simple models of equilibrium vaporization.

(5) There were changes in the relative production rates with heliocentric distance.

(a) The comet was CN-rich at discovery ($r_H = 0.57$ AU).

(b) Abundance ratios were normal and nearly constant for $0.6 < r_H < 1.0$ AU.

(c) OH and C_2 gradually decreased relative to CN and C_3 for $r_H > 1.0$ AU.

(d) The production of C_2 peaks, relative to CN, at $r_H \sim 1.0$ AU.

We thank M. P. Candy for his assistance both in the observing and in providing ephemerides, and we also thank J. Johnson, I. Nikoloff, and D. T. Thompson for assistance with the observations. We are indebted to P. D. Feldman and M. C. Festou for numerous helpful discussions both regarding the comparison between the ground-based data and the IUE data and also regarding atmospheric extinction for the OH observations. We are also indebted to L. Dunkelman for helpful discussions regarding the latter point. This work was supported at the University of Maryland by NASA Grant No. NSG 7322 and at Lowell Observatory by NASA Grant No. NGR 03-003-001.

REFERENCES

A'Hearn, M. F. (1981). In *Comets: Gases, Ices, Grains, and Plasmas*, edited by L. Wilkenning (in press).
A'Hearn, M. F., and Cowan, J. J. (1980). Moon and Planets **23**, 41.
A'Hearn, M. F., Hanisch, R. J., and Thurber, C. H. (1980). Astron. J. **85**, 74.
A'Hearn, M. F., and Millis, R. L. (1980). Astron. J. **85**, 1528.
A'Hearn, M. F., Millis, R. L., and Birch, P. V. (1979). Astron. J. **84**, 570.
A'Hearn, M. F., Thurber, C. H., and Millis, R. L. (1977). Astron. J. **82**, 518.
Allen, C. W. (1963). *Astrophysical Quantities*, 2nd ed. (Athlone, London), p. 127.
Breger, M. (1976). Astrophys. J. Suppl. **32**, 1.
Brin, G. D., and Mendis, D. A. (1979). Astrophys. J. **229**, 402.
Code, A. D., and Meade, M. R. (1979). Astrophys. J. Suppl. **39**, 195.
Combi, M. R. (1978). Astron. J. **83**, 1459.
Combi, M. R., and Delsemme, A. H. (1980a). Astrophys. J. **237**, 633.
Combi, M. R., and Delsemme, A. H. (1980b). Astrophys. J. **237**, 641.
Cowan, J. J., and A'Hearn, M. F. (1979). Moon and Planets **21**, 155.
Despois, D., Gerard, E., Crovisier, J., and Kazes, I. (1979). Paper presented at IAU General Assembly 17, Commission 15, Montreal, August 1979.
Festou, M. C. (1981a). Astron. Astrophys. **95**, 69.
Festou, M. C. (1981b). Astron. Astrophys. **96**, 52.
Giguere, P., and Huebner, W. (1978). Astrophys. J. **223**, 638.
Hayes, D. S., and Latham, D. W. (1975). Astrophys. J. **197**, 593.
Huebner, W. F. (1981). In *Comets and the Origin of Life*, edited by C. Ponnamperuma (in press).
Hunnaerts, J. (1953). Mem. Soc. R. Sci. Liege, 14th Ser. **13**, 59.
Levin, B. J. (1966). Mem. Soc. R. Sci. Liege, 15th Ser. **12**, 65.
Marcus, J. M. (1980). Comet News Service, No. 80-2.
Millis, R. L., and A'Hearn, M. F. (1981). In *Workshop on Modern Observational Techniques for Comets*, edited by J. C. Brandt (in press).
Mitchel, G. F., Prasad, S. S., and Huntress, W. T. (1981). Astrophys. J. **244**, 1087.
Morris, C. S. (1980). Int. Comet Q. **2**, 24.
Öpik, E. J. (1963). Ir. Astron. J. **6**, 93.
Schleicher, D. G., and A'Hearn, M. F. (1981). Submitted to Astrophys. J.
Tatum, J. B., and Gillespie, M. I. (1977). Astrophys. J. **218**, 569.
Toolin, R. B. (1965). In *Handbook of Geophysics and Space Environments*, edited by S. L. Valley (A. F. Cambridge Research Lab, Bedford, Mass.), Chap. 7.
Weaver, H. A., Feldman, P. D., Festou, M. C., and A'Hearn, M. F. (1981). Astrophys. J. (in press).
Whipple, F. L. (1978). Moon and Planets **18**, 343.